

# A Novel Technology for Simultaneous Tensile Loading and High-Resolution Imaging of Cells

BAO-NGOC B. NGUYEN,<sup>1</sup> JOSHUA CHETTA,<sup>1</sup> and SAMEER B. SHAH<sup>1,2</sup>

<sup>1</sup>Fischell Department of Bioengineering, University of Maryland, College Park, MD, USA; and <sup>2</sup>Departments of Orthopaedic Surgery and Bioengineering, University of California, San Diego, 9500 Gilman Drive, Mail Code 0863, La Jolla, CA 92093, USA

(Received 25 January 2012; accepted 23 July 2012; published online 10 August 2012)

Associate Editor Joyce Wong oversaw the review of this article.

**Abstract**—A variety of methods have been used to study the tensile properties of cells or the influence of tensile loading on cellular function. Such methods are frequently limited either by cellular detachment or by an inability to image cells at high temporal or spatial resolution. Previously, we preserved cellular adhesion during loading and imaging by using a flexible silicone membrane inverted over a glass coverslip. This enabled high magnification real-time imaging of sub-cellular structures but chemical and physical access to the cells was limited due to geometric constraints. In this study, we present a method to integrate thin films made from poly(dimethylsiloxane) (PDMS) into a novel device. The optically clear PDMS thin films allow simultaneous tensile loading and high magnification microscopy without the need to invert the cells, maintaining physical access during experiments. To characterize the utility of this technology, we evaluated fabrication conditions for optimizing the geometry, durability, and uniformity of these films. Additionally, we demonstrate the suitability of this device for use in high-magnification, live-cell fluorescence microscopy by examining the response of the cytoskeletal protein actin, expressed in cultured primary sensory neurons, to a tensile load. This technology offers considerable potential for extending our understanding of mechanical influences on cellular function at a variety of spatial and temporal scales.

**Keywords**—Tensile loading, PDMS, Thin film, Flexible substrate, Cell mechanics, Neuronal cytoskeleton.

## INTRODUCTION

The morphology and function of numerous cell types are strongly influenced by their mechanical environment.<sup>52,57</sup> Imposed mechanical loads may be broadly categorized as tensile, compressive, or shear.

Tensile loading, or stretch, has been implicated in a wide range of cellular activities, including differentiation, migration, definition of cell morphology, cytoskeletal remodeling, and gene and protein expression.<sup>2,15,19,45,60</sup>

A variety of experimental systems have been developed to study the tensile properties of cells and their response to applied tension. One class of approaches has employed calibrated glass micropipettes, optical tweezers, or magnetically controlled flexible microposts to regionally deform or measure viscoelastic properties of single cells.<sup>13,22,36,47,50,61</sup> Such strategies have also been scaled up to accelerate the outgrowth of tracts of neuronal projections by means of a sliding glass plate housed within a bioreactor.<sup>35,42</sup> However, these strategies require full or partial detachment of the stretched cells from their substrate, which can adversely influence cell motility.

Alternately, deformation of a flexible culture substrate such as silicone or acrylamide enables the tensile loading of adherent cells. A popular commercial device utilizes a vacuum chamber to apply, in its simplest configuration, a radial deformation to a flexible substrate.<sup>16</sup> Additional inserts can be used to adapt the chamber to apply a uniaxial load. Several groups have also applied equibiaxial or uniaxial loading to flexible substrates using clamps coupled to actuators or moving stages.<sup>3,4,23,28,55</sup> Though a small number of research groups have successfully integrated mechanical loading with high resolution upright microscopy through water immersion lenses,<sup>27,32,53</sup> the thickness and opacity of the utilized substrates preclude high resolution imaging using inverted microscopy.<sup>58</sup>

An alternative method aimed at preserving cellular adhesion during loading and imaging is to invert cells seeded on a flexible silicone sheet suspended over a glass coverslip.<sup>10,18,56</sup> The silicone sheet and adherent cells must be brought close enough to the coverslip to

Address correspondence to Sameer B. Shah, Departments of Orthopaedic Surgery and Bioengineering, University of California, San Diego, 9500 Gilman Drive, Mail Code 0863, La Jolla, CA 92093, USA. Electronic mail: sbshah@ucsd.edu

B.-N. B. Nguyen and J. Chetta contributed equally to this work.

be within the working distance of a high-magnification microscope objective, which is typically less than 200  $\mu\text{m}$  for 40 $\times$  or 60 $\times$  objectives. This configuration is conducive to imaging subcellular structures, but physical access to the cells, for solution exchange, localized drug delivery or localized mechanical perturbation, is severely limited.

Overcoming these limitations would significantly advance efforts to understand the effects of tensile loading on cellular function. One solution is the implementation of an optically clear and flexible substrate compatible with conventional microscopy techniques that would preclude the need to invert cells. In order to achieve this, a film would need to be thin enough that adherent cells on its surface would still be within the working distance of a high magnification microscope objective, yet robust enough to withstand being stretched at typical strain rates ( $\leq 0.03\%/s$ ) usually employed during these types of experiments.<sup>42,49</sup>

To meet these criteria, we incorporated thin films made from poly(dimethylsiloxane) (PDMS) into a system in which cells can be imaged at high magnification during exposure to an applied uniaxial tensile load without substrate inversion. PDMS is a relatively inexpensive, optically clear, and biocompatible silicone elastomer that has been widely used in the development of microfluidic systems.<sup>14,46</sup> Methods of varying complexity have been used to create thin films from PDMS, including micropatterning,<sup>8,41,43</sup> replica modeling,<sup>9,38</sup> and spin-casting.<sup>23</sup> Thus far, however, these films have not been transferred from the fabrication substrate to another device, and therefore their utility in tensile loading is not known.

In this study, we tested a number of casting protocols to optimize the material properties and thickness profile of thin PDMS films. We demonstrate that uniaxial strains are distributed uniformly across the surface of PDMS films, and we present results from experiments using this technology for high-resolution, live-cell tracking of the movement of GFP-actin within the axon of a cultured sensory neuron before and after an applied tensile load.

## METHODS

### *Thin Film Fabrication*

$\frac{1}{4}$  inch thick polycarbonate plates were fabricated into either 15 cm squares or 15 cm diameter circles. These were used as spinning substrates to evaluate the material characteristics of films cast onto the two different geometries. PDMS (Sylgard 184 Elastomer Kit, Dow Corning) was mixed using a standard 10:1 base to curing agent ratio. 4 g of the liquid PDMS was placed on the center of each polycarbonate substrate and spun

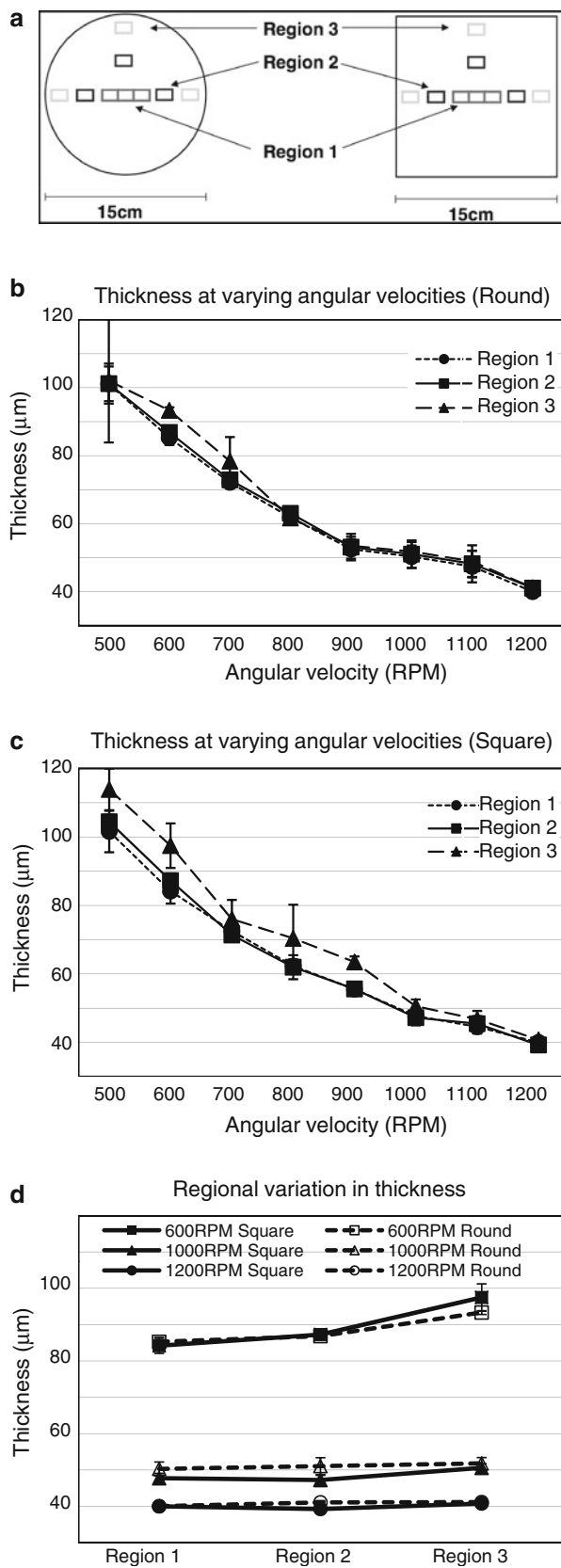
for 60 s at a range of 500–1200 rpm in a clean room setting. The films were cured for 3 h at 70  $^{\circ}\text{C}$  or overnight at room temperature, based on published curing curves.<sup>54</sup> The films were then cut into 90 cm  $\times$  30 cm “imaging sheets” with a razor blade and sterilized with ethanol before use as a flexible culture substrate in the cell-stretching device.

### *Thin Film Characterization*

A Tencor TP-20 profilometer was used to measure the thickness profile of the cured PDMS films. Nine 1 cm  $\times$  0.5 cm samples from both the circular and square plates were measured. Three samples were taken from each of three regions and the average thickness of each region was calculated (Fig. 1a). To evaluate the feasibility of using cured PDMS thin films as a flexible culture substrate, resistance to tearing and ease of handling were both evaluated. To measure the susceptibility of the PDMS films to damage during tensile loading, the 90 mm  $\times$  30 mm imaging sheets were clamped on either end leaving a 60 mm long region between the clamp, similar to the configuration of the sheet within the cell stretching device. The PDMS was then stretched until failure at a rate of 0.03–0.04%/s, and the maximum strain was recorded. Sheets were also evaluated for how easily they could be removed from the polycarbonate spin plates and loaded onto the stretcher. During removal, films transiently experienced strain rates estimated to be a maximum of  $\sim 0.1\%/s$ . Table 1 defines the scoring systems that were used to evaluate these properties.

### *Tissue Culture*

The University of Maryland Institutional Animal Care and Use Committee approved all animal experiments. Dorsal Root Ganglia (DRG) were isolated from the entire spinal column of 2–5 day old Sprague–Dawley rats and maintained in ice cold F-10 supplemented with gentomycin. After removal from the spinal column, whole DRGs were incubated with 2.5 mg/mL collagenase II (Roche, Basel, Switzerland) for 15 min at 37  $^{\circ}\text{C}$ , pelleted at 76 $\times$ g for 5 min, triturated in F-10, and pelleted again. Following protocols provided by the manufacturer, dissociated cells were then resuspended in electroporation media with 3 mg/mL of plasmid encoding GFP-actin and immediately electroporated using an Amaxa Nucleofector II (Lonza, Walkersville, MD). After electroporation they were allowed to recover for 20 min in RPMI at 37  $^{\circ}\text{C}$  before being resuspended in growth media (10% Horse Serum in F-10 media, with 1% penicillin/streptomycin, 1% L-glutamine), seeded onto sterilized, laminin-coated PDMS films at a density of 100,000–



◀ **FIGURE 1.** Thickness of PDMS films is dependent on angular velocity, but not substrate shape or location on the substrate. (a) Regions of measured PDMS on circular and square polycarbonate substrates. Samples were taken from the center (Region 1), middle (Region 2), and edge (Region 3) of round or square-shaped plates. (b) Average thickness of PDMS films as a function of angular velocity and distance from the center of round substrates. Curves were regressed with a power law. Region 1:  $\alpha = 0.44$ ,  $k = 109.4$ ,  $R^2 = 0.96$ ; Region 2:  $\alpha = 0.43$ ,  $k = 109.9$ ,  $R^2 = 0.96$ ; Region 3:  $\alpha = 0.45$ ;  $k = 114.6$ ,  $R^2 = 0.94$ . (c) Average thickness of PDMS films as a function of angular velocity and distance from the center of square substrates. Curves were regressed with a power law. Region 1:  $\alpha = 0.45$ ,  $k = 110.6$ ,  $R^2 = 0.96$ ; Region 2:  $\alpha = 0.47$ ,  $k = 113.8$ ,  $R^2 = 0.97$ ; Region 3:  $\alpha = 0.49$ ;  $k = 127.2$ ,  $R^2 = 0.94$ . (d) Direct comparison of differences in thickness in different regions of square vs. round substrates for angular velocities of 600, 1000, and 1200 rpm. No statistically significant differences were found between the thickness at a particular angular velocity and region on square and round substrates.

250,000 cells/mL, and incubated at 37 °C and 5% CO<sub>2</sub> for 16–20 h.

#### Cell Stretching Apparatus

Previously, we developed a cell stretching device to image cells during tensile loading.<sup>10</sup> In this original configuration, a flexible silicone membrane was clamped at a fixed length under minimal tension. Cells were seeded onto this substrate and maintained in a cell culture incubator to allow cell adhesion and growth. The clamp-substrate apparatus was then inverted and loaded into a custom-designed glass-bottomed chamber for uniaxial stretch and simultaneous imaging. In the current study, cells were seeded onto clamped PDMS films and allowed to adhere and grow overnight. The clamped PDMS apparatus was then loaded upright into the glass-bottomed chamber for stretch and imaging.

#### Imaging and Biomechanics Protocols

Microscopy was performed on an inverted TE-2000E microscope (Nikon, Melville, NY) outfitted with a LumenPRO2000 (Prior Scientific, Rockland, MA) illumination system, 10 $\times$  or 40 $\times$  objectives, and filters appropriate for FITC or GFP (Chroma, Bellows Falls, VT. EPI: 488 nm, Emission 530 nm). Additionally, a custom built chamber (Precision Plastics, Beltsville, MD) maintained optimal temperature, humidity and CO<sub>2</sub> levels during imaging of live cells. Exposure time was limited to 200–300 ms per image.

To determine the uniformity of the strain in the PDMS film, 200 nm fluorescent beads (Invitrogen, Carlsbad, CA) were allowed to settle and images were taken before and after 5 or 10% strain within central regions of the sheet. The change in position of these

**TABLE 1. Scoring criteria for tendency to fail and manipulability.**

	Failure analysis	Ease of use
1	Failure during handling/clamping	Very difficult to use → breaks right away/extremely sticky, cannot be lifted off of substrate
2	Withstands <5% strain	Difficult to use → breaks easily and is sticky
3	Withstands 5–10% strain	Slightly difficult to use → minor tearing
4	Withstands 10–20% strain	Easy to use → rare tearing and not sticky
5	Withstands >20% strain	Very easy to use → no tearing and not sticky

beads after the applied stretch was used to calculate strain.

For cell imaging and mechanics, protocols were similar to those published previously.<sup>10</sup> Briefly, axons chosen for analysis were oriented in the direction of the applied strain ( $\pm 15^\circ$ ), were not in contact with other cells, and were in a non-growing state. Cellular and cytoskeletal response was evaluated in two phases. For the first “instantaneous” phase, three paired (DIC and fluorescence) images were taken of the unstretched (0% strain) cells with a 30 s lapse between each image. These images were used to confirm that puncta of actin used to calculate instantaneous strain were indeed stationary. The cells were then exposed to a 10% strain applied at a rate of 0.03%/s, after which 3 more paired images were captured. For the second “sustained deformation” phase, deformed cells were continued to be imaged over the course of 6 min with fluorescent images captured every 5 s, to assess longer term changes in the distribution and movement of actin following the application of strain.

#### *Image Processing and Kymograph Analysis*

All image analysis was performed in ImageJ (NIH, Bethesda, MD) or MATLAB (The MathWorks, Natick, MA). For beads, the  $x$  and  $y$  coordinates of adherent beads before and after stretch were determined within several imaging fields, to calculate regional variability in strain. In addition, a computational deformation of 10% was imposed on the “before” image, to determine the distribution of beads following perfectly homogeneous deformation. For cells, we followed previously established protocols.<sup>10</sup> For the instantaneous loading phase, the distance between a pair of stationary actin puncta, as defined above, was determined for both 0% (unstretched) and 10% applied strain and used to calculate the strain in the intervening space. Strain was defined as the change in separation between puncta divided by the initial separation, or  $\Delta l/l_0$ . In addition, two points that flanked the region of fluorescence analysis were used to calculate whole axon strain, from DIC images corresponding to 0 and 10% stretch. For

the sustained deformation phase, kymographs of actin movement were captured from the timelapse movies. Briefly, a line segment of pixel intensities along the axon was produced for each time point.<sup>11</sup> The position of each punctum was then manually extracted from these kymographs and used to calculate mobility parameters of non-stationary particles as well as strain between initially stationary particles over time.

#### *Statistical Analysis*

Statistical analysis was performed using Excel (Microsoft, Seattle, WA). Linear regression was used to examine relationships between measured substrate strain and the relative position of markers used to measure this strain. A power law was used to regress relationships between angular velocity,  $\omega$ , and the thickness of PDMS films,  $t$ , in the form  $t = k\omega^{-\alpha}$  where  $k$  and  $\alpha$  are fit parameters.<sup>30,31,40</sup> Means were compared using a two-tailed  $t$  test, assuming unequal variances.

## RESULTS

### *Fabrication and Characterization of PDMS Films*

We first examined the relationship between angular velocity and thickness for thin films of PDMS spun onto smooth polycarbonate plates of two geometries. Round plates were examined due to their radial symmetry around the site of polymer deposition prior to spinning, and square plates were examined because more rectangular imaging sheets could be cut from each plate compared to circular plates.

The thickness of regions in the center, middle, and edge of films spun at varying speeds (Fig. 1a) were measured using a profilometer. On both round and square plates, the thickness of the PDMS film, as expected, decreased with increased angular velocity to a minimum thickness of  $\sim 40 \mu\text{m}$  at 1200 rpm (Figs. 1b and 1c). A power law accurately described this relationship, with  $\alpha = 0.43\text{--}0.45$  ( $r^2 > 0.93$  in all regions) on round plates (Fig. 1b) and  $\alpha = 0.45\text{--}0.49$  ( $r^2 > 0.94$  in all regions) on square plates (Fig. 1c). Two-way

ANOVA revealed a significant effect of angular velocity ( $p < 0.01$ ), but no significant effect of substrate geometry on film thickness. An angular velocity of 500 rpm resulted in considerable variability in film thickness on plates of both geometries. Above this speed, some subtle differences emerged, particularly at the edge regions; the thickness of films spun on round plates appeared to be slightly less variable at velocities below 900 rpm compared to films spun on square substrates. In contrast, films on square plates were more homogeneous when spun at velocities of 1000 rpm or higher. To test whether these differences were significant, we directly compared a range of angular velocities, corresponding to thicknesses potentially appropriate for high-resolution imaging, for plates of both geometries (Fig. 1d). No significant differences were observed, suggesting that both round and square plates were likely to be suitable for film preparation. For subsequent analysis, we used films spun onto round substrates.

We next examined the durability and manipulability of PDMS films. While the tensile properties of PDMS films are well characterized for a range of thicknesses,<sup>1,34</sup> our assessment provided a more practical assessment of ease of handling and consistency from film to film. Based on criteria described in Table 1, results are summarized in Table 2. Surprisingly, the thickest PDMS films, spun at angular velocities of less than 800 rpm, were more difficult to handle and stretch; they were extremely adherent to themselves and other objects during removal from the substrate and mounting within test devices. PDMS films spun at 900 and 1000 rpm were significantly easier to handle and were more durable compared to those spun at lower speeds. Films spun at 1100 or 1200 rpm were again more fragile, most likely as a consequence of their reduced thickness.

Based on these data, we elected to use films spun at an angular velocity of 1000 rpm. These films were thin enough to be within theoretical focal distances of high

magnification objectives, but durable enough to reliably bear tensile loads. To evaluate the consistency and homogeneity of strain in stretched films, we seeded polystyrene beads on a laminin-coated sheet and determined bead position before and after an imposed 5% (Fig. 2a) and 10% strain, which was calculated based on the clamp-to-clamp distance. Qualitatively, it is apparent from the beads at the edges of the imaging field that a longitudinal strain was imposed. We also compared the positions of beads on the experimentally deformed membrane with those on the image of the unstretched film subject to a 2-D computational deformation of 5% longitudinally and 3% laterally (Fig. 2b). There is strong agreement between the experimental and theoretical deformation.

Using such images, we then quantified the homogeneity of deformation. Longitudinal strain was calculated based on the before and after positions of at least 15 pairs of beads visible in each image. This strain was plotted against the angle between the beads; beads in line with each other along the axis of deformation had an angle of 0°, while beads oriented perfectly perpendicular to the axis of deformation had an angle of 90°. There was considerable deviation from the expected 10% strain at higher angles (Fig. 2c) due to the propagation of edge effects induced by uniaxial clamping of the membrane. However, when analysis was restricted to angles within  $\pm 25^\circ$  of the axis of deformation, i.e., points along the axis of deformation, strains were far more uniform and predictable, with a regression slope of essentially zero (5%: slope =  $-0.0003$ ,  $r^2 = 0.93$ ; 10%: slope =  $-0.0001$ ,  $r^2 = 0.37$ ; Fig. 2d). Interestingly, measured strains were consistent, but slightly overshot the predicted 10 and 5% deformations ( $Y$ -intercepts = 0.117 (11.7%) and 0.062 (6.2%), respectively).

Finally, we examined whether the fabricated thin films were suitable for cellular imaging and yielded images of high quality for subsequent image processing. Primary sensory neurons electroporated with a plasmid encoding GFP-actin successfully extended axons on laminin-coated films. Morphology appeared consistent with that of neurons seeded on glass or silicone, and both DIC and fluorescence images were in focus, with morphological features or fluorescence puncta clearly visible (e.g., Fig. 3a). We then evaluated cellular response immediately after 10% strain (phase 1, Figs. 3a and 3b) and during maintenance of this 10% strain (phase 2, Fig. 3c). The imposed 10% strain yielded an instantaneous cellular strain of  $\sim 8\%$ , measured based on the deflection of extracellular fiduciary markers visible on DIC images before and after strain (Figs. 3a and 3b). However, based on the deflection of additional extracellular (DIC) and intracellular (fluorescence) markers, there was considerable regional variability in deformation. This was possibly due to

**TABLE 2. Scoring of the tendency to fail and manipulability of PDMS films.**

Angular velocity (rpm)	Failure analysis	Ease of use score
500	1.00 $\pm$ 0.00	1.00 $\pm$ 0.00
600	1.00 $\pm$ 0	2.00 $\pm$ 0.00
700	2.00 $\pm$ 0.00	2.00 $\pm$ 0.00
800	3.66 $\pm$ 0.33	2.66 $\pm$ 0.33
900	4.33 $\pm$ 0.33	4.66 $\pm$ 0.33
1000	5.00 $\pm$ 0.00	4.66 $\pm$ 0.33
1100	3.00 $\pm$ 0.00	4.33 $\pm$ 0.33
1200	2.33 $\pm$ 0.33	2.33 $\pm$ 0.33

Data is presented as (mean  $\pm$  SEM) and is based on criteria in Table 1.

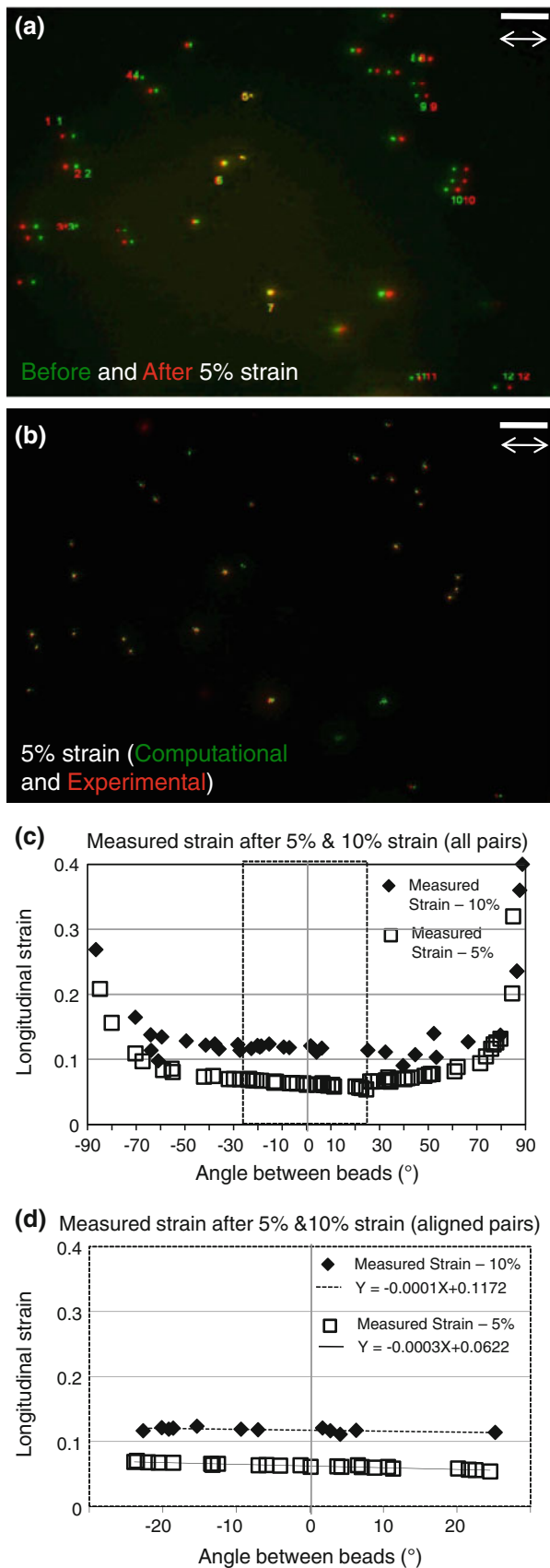


**FIGURE 2.** Longitudinal deformation on thin PDMS films is homogeneous. (a) Fluorescent beads on a PDMS film spun at 1000 rpm before (green) and after 5% strain (red). Note that on the left side of the image, red beads are to the left of the green beads, while on the right side of the image, red beads are to the right of the green beads, indicating deformation. Before and after images were aligned at the vertical midline, as apparent from yellow (overlapping) beads near this region. Bar = 100  $\mu\text{m}$ . Arrows indicate the direction of longitudinal loading. (b) Fluorescent beads on PDMS subject to a computational (green) and experimental (red) longitudinal strain of 5% and lateral strain of 3%. Note that there is strong alignment from right to left, in the direction of the deformation (right and left) and laterally (up and down). Bar = 100  $\mu\text{m}$ . Arrows indicate the direction of longitudinal loading. (c) Measured strain for pairs of beads as a function of the angle separating them within an entire imaging field for 5 and 10% imposed strain.  $0^{\circ}$  corresponds to horizontal (direction of deformation) and  $\pm 90^{\circ}$  corresponds to vertical (perpendicular to axis of deformation). Dotted box indicates region corresponding to beads aligned within  $\pm 25^{\circ}$  of the direction of stretch. This region of the graph is amplified in “d”. (d) Region corresponding to the dotted box in “c”. Data within this region for 5 and 10% strain have been fit with a linear regression line.

interactions of branch points or other sites of adhesion to the substrate before strain and straightening of axonal regions slightly deviating from the axis of stretch. Kymograph analysis was then used to track actin mobility during the sustained 10% strain. Fluorescence trajectories revealed a dense fluorescence field similar in quality and pattern to GFP-actin trajectories observed previously on glass substrates.<sup>11</sup> Within this image, 84 distinct puncta were traced and quantitatively analyzed for characteristics such as directional movement (Fig. 3d), velocity, and run length (Fig. 3e). The biological significance of such transport profiles following substrate strain will be examined in a future study; however, the ability to generate such profiles at high spatial and temporal resolution demonstrates the feasibility of the methodology, even for dense and complex particle fields.

## DISCUSSION

We have described the fabrication and characterization of a novel cell-stretching device that enables simultaneous tensile loading and high-resolution cellular imaging. We have also demonstrated the feasibility and suitability of this device for use in high-resolution, live-cell fluorescence microscopy. In particular, based on our interest in mechanical determinants of neuronal function,<sup>6,10</sup> we have initially used our device to examine the response of cultured sensory neurons expressing a fluorescent cytoskeletal protein to mechanical loading.

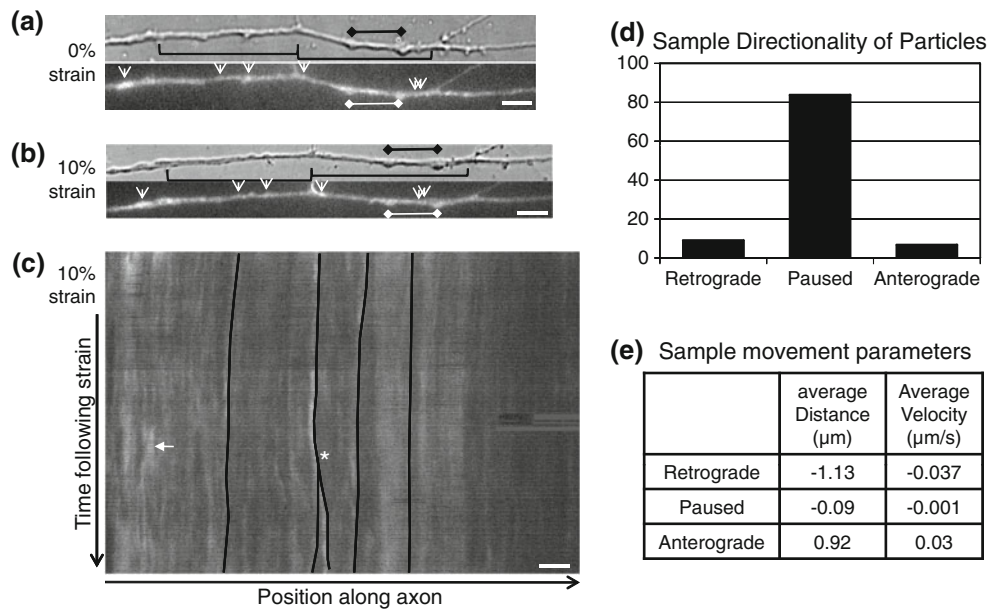


**FIGURE 3.** Brightfield and fluorescence images are clearly visible at high resolution through thin PDMS films. (a–b) DIC and fluorescence images of a sensory (DRG) axon before (a) and after (b) 10% deformation of the substrate. Overall strain in the axon is ~8%, based on the deformation of markers in the DIC images. However, based on the deflection of extracellular (DIC) and intracellular (fluorescence) markers, there is considerable regional variability in deformation, possibly due to interactions of branch points or other sites of adhesion to the substrate before strain as well as regional straightening of axonal regions slightly deviating from the axis of stretch. Prongs of black brackets indicate extracellular markers, including branch points, used to calculate cellular strain. White arrowheads indicate intracellular GFP-actin puncta that could be tracked before and after strain, to estimate cytoskeletal strain. Black and white diamond-tipped lines indicate a region of the axon that did not appear to stretch at all, based on an unchanged distance between both extracellular and intracellular markers. Bar = 10  $\mu\text{m}$ . (c) Kymograph indicates position of GFP-actin puncta over time. Four such puncta are indicated by black lines, which are positioned just to the right of the actual trajectory. The anterograde direction (away from the cell body) is oriented towards the right; the retrograde direction (towards the cell body) is oriented towards the left. Resolution is sufficient to detect subtle changes in direction as well as branching (asterisk) and convergence or crossing (arrow) of tracks, which result in a reduction or spike in fluorescence, respectively. Bar = 10  $\mu\text{m}$ . (d) Sample analysis of tracks contained in “c” ( $n = 84$  distinct puncta). Stationary particles were designated based on a net velocity less than 0.002  $\mu\text{m/s}$  over the course of the movie. (e) Sample movement profiles of anterograde, retrograde, and stationary particles. Note that distances and velocities for stationary particles were calculable from raw data, and reflect a subtle directional drift.

### Comparison to Previous Tensile Loading Strategies

The dynamics of subcellular structures have been imaged at high resolution following a number of mechanical perturbations to cells cultured on glass substrates.<sup>23,25,33</sup> Tensile loads in particular have been imposed on detached or partially detached cells and tissues by methods including calibrated glass micropipettes, optical tweezers, uniaxial clamps, or magnetically controlled flexible microposts.<sup>13,22,33,36,42,44,47,49–51,61</sup> Adherent cells have been stretched by flexing their substrate by means of indentation or pressure.<sup>16,24,48</sup> Others have deformed clamped, flexible substrates directionally through the use of actuators.<sup>7,17,24,29,39,48</sup> A major shortcoming of these strategies is the inability to image subcellular cellular response at high magnification using inverted microscopy. Cell outlines or larger subcellular structures, such as nuclei or larger stress fibers, may be imaged through thicker substrates, but finer structures are masked. A few groups have addressed this issue by using high-resolution upright microscopy.<sup>27,32,53</sup> Alter-

nately, we and others have inverted flexible substrates in close proximity to a coverslip<sup>10,56</sup>; however, substrate inversion restricts chemical and physical access to cells, somewhat limiting its utility.

By integrating an optically clear, durable, and predictably deformable thin PDMS film into a tensile loading device, we have eliminated the need for substrate inversion while allowing cellular adhesion during loading. In addition to the simplicity of our fabrication protocol, our incorporation of PDMS into the device offers additional advantages. PDMS has already been extensively used for a wide range of biological applications, reducing concerns about biocompatibility.<sup>12,26,46</sup> In fact, a PDMS film has previously been used for tensile loading of cells,<sup>23</sup> though it was too thick for high-resolution imaging. In addition, the ability to easily manipulate the material properties of and micropattern PDMS<sup>26,37</sup> greatly enhances the ability to customize experimental applications of the device. It should be noted that relatively thin (100–

200  $\mu\text{m}$ ) silicone or PDMS films are commercially available, and a pre-strain may be imposed to obtain films thin enough for high-resolution imaging. However, prestrain may induce unexpected or unpredictable differences in mechanical properties, cell adhesion, orientation, and locomotion,<sup>5,20,21</sup> potentially due to strain-induced wrinkling or nano-scale substrate reorganization. Additionally, due to the propagation of edge effects, imposing an additional 10–20% strain on an already strained membrane may result in increased susceptibility to damage.

#### *Fabrication and Characterization of Thin PDMS Films*

An appropriately thin PDMS film of predictable and uniform thickness is required for repeatable cellular deformation and simultaneous imaging. Angular velocities between 500 and 1200 rpm yielded films less than 100  $\mu\text{m}$ , with those exceeding 800 rpm exhibiting uniform thickness (Fig. 1). We, like several groups, observed a clear power law relationship between angular velocity and PDMS thickness, confirming control over film geometry. Our  $\alpha \approx 0.4$  accurately described this relation for films spun at speeds of 500–1200 rpm for 1 min. This value is similar to the value of  $\alpha \approx 0.5$  observed by numerous groups under a wide range of spin conditions (reviewed in Norrman et al.<sup>40</sup>). However, the slightly lower value may reflect low levels of fluid inertia.<sup>31</sup> It should be noted that solvent and spin duration may also considerably influence  $\alpha$ . Our value deviates significantly from  $\alpha \approx 0.98$  described for PDMS spun at higher speeds (1000–6000 rpm) for durations of  $> 5$  min.<sup>30</sup>

Our intended integration of films into a cell-stretching device required several additional practical design criteria for fabrication. Thin PDMS films are frequently used to coat a substrate, in which case they may be spun directly and irreversibly on their substrate. Alternately, PDMS itself may be used to lift off thin PDMS films from their substrate.<sup>59</sup> In contrast, here, the films needed to be removed from the casting substrate as a sheet before being mounted within the loading device; consequently, they needed to be durable and easy to handle. The thickest films were quite fragile and difficult to use owing to their adhesiveness (Table 2). Though the exact reason for this is unclear, it may be that slower angular velocities resulted in an increased probability of internal defects within polymerized sheets as well as increased variability in thickness (Fig. 1). Films spun at greater than 1000 rpm were the thinnest but were also very fragile. Therefore, only films spun at speeds between 900 and 1000 rpm, corresponding to thicknesses between 45 and 50  $\mu\text{m}$ , were usable. A final design criterion for fabrication

addressed the potential scalability of fabrication. Ideally, a single spin would yield material for several experiments. Because PDMS membranes mounted within the mechanical loading device are rectangular, a square casting plate would maximize usage of material. Differences between films spun on square and round plates were minimal but slight edge effects were apparent on square plates at high angular velocities, warranting some caution (Fig. 1d).

Following the above characterization, we ultimately elected to use films spun at 1000 rpm as a circular substrate. Based on comprehensive measurement of bead positioning before and after 5 and 10% strain, we confirmed that the distribution of strains on films following mechanical loading was predictable along the axis of deformation (Fig. 2). We tested specimens at maximum strain rates of 0.03%/s, which are typical for substrate deformation studies. However, given the importance of strain rates on the biomechanical and physiological viscoelastic response of a cell, the performance of films at higher strain rates should be examined as needed. The slight overshoot of measured strain compared to the applied strain was likely a propagation of edge effects from the clamps. Strains were also suitably transmitted to cells; measured axonal strains were only  $\sim 80\%$  of substrate strain (Figs. 3a and 3b), but this value exceeds typical reported strains of 30–60% for cells on other substrates.<sup>4,55</sup> Both this undershoot of cell strain compared to substrate strain and any regional heterogeneity within single cells (Fig. 3b) are likely to be a result of variability in cellular adhesive and structural components,<sup>10</sup> rather than heterogeneity of substrate deformation.

The predictability of deformations imposed longitudinally was ideal to study cells polarized relative to the axis of stretch, including neuronal projections. Therefore, we tested the quality of images acquired through the PDMS film by probing the axonal movement of fluorescently labeled actin, a cytoskeletal cargo of exceptional complexity due both to high background levels and to its subtlety of movement. The biological significance of the reorganization of actin in response to tensile loading is outside the scope of this methodological study, but the fact that we were able to accurately extract meaningful motility parameters speaks to the high quality of imaging and highlights the significant value of this system.

## CONCLUSIONS

Through the careful characterization of our novel cell-stretching device, we confirmed its utility for examining cellular response to tensile loading. Though



the system was validated using cultured neurons, this technology has applicability for any number of cells that are responsive to tensile loads for alignment, motility, differentiation, signaling, or gene expression. This broad applicability is further enhanced by the versatility of PDMS. Indeed, one can envision the integration of patterned substrates of varying material properties into experimental design, or even the possibility of manufacturing disposable flexible chambers themselves out of PDMS. Ultimately, this technology offers considerable potential for extending our understanding of mechanical influences on cellular function at a variety of spatial and temporal scales.

### ACKNOWLEDGMENTS

We gratefully acknowledge technical assistance by staff of the Maryland Nanocenter Micro and Nano Fabrication Laboratory and helpful discussions with the Neuromuscular Bioengineering Laboratory. This research was supported by funding from the National Science Foundation (CBET0932590 and CMMI1130997) and the State of Maryland Stem Cell Research Commission.

### REFERENCES

- <sup>1</sup>Armbruster, C., M. Schneider, S. Schumann, K. Gamberdinger, M. Cuevas, S. Rausch, G. Baaken, and J. Guttmann. Characteristics of highly flexible pdms membranes for long-term mechanostimulation of biological tissue. *J. Biomed. Mater. Res. B* 91:700–705, 2009.
- <sup>2</sup>Baker, B. M., R. P. Shah, A. H. Huang, and R. L. Mauck. Dynamic tensile loading improves the functional properties of mesenchymal stem cell-laden nanofiber-based fibrocartilage. *Tissue Eng. A* 17:1445–1455, 2011.
- <sup>3</sup>Barbee, K. A., E. J. Macarak, and L. E. Thibault. Strain measurements in cultured vascular smooth muscle cells subjected to mechanical deformation. *Ann. Biomed. Eng.* 22:14–22, 1994.
- <sup>4</sup>Bieler, F. H., C. E. Ott, M. S. Thompson, R. Seidel, S. Ahrens, D. R. Epari, U. Wilkening, K. D. Schaser, S. Mundlos, and G. N. Duda. Biaxial cell stimulation: a mechanical validation. *J. Biomech.* 42:1692–1696, 2009.
- <sup>5</sup>Bischofs, I. B., and U. S. Schwarz. Cell organization in soft media due to active mechanosensing. *Proc. Natl. Acad. Sci. USA* 100:9274–9279, 2003.
- <sup>6</sup>Bueno, F. R., and S. B. Shah. Implications of tensile loading for the tissue engineering of nerves. *Tissue Eng. Part B Rev.* 14:219–233, 2008.
- <sup>7</sup>Caille, N., Y. Tardy, and J. J. Meister. Assessment of strain field in endothelial cells subjected to uniaxial deformation of their substrate. *Ann. Biomed. Eng.* 26:409–416, 1998.
- <sup>8</sup>Camelliti, P., A. D. McCulloch, and P. Kohl. Microstructured cocultures of cardiac myocytes and fibroblasts: a two-dimensional in vitro model of cardiac tissue. *Microsc. Microanal.* 11:249–259, 2005.
- <sup>9</sup>Cesa, C. M., N. Kirchgessner, D. Mayer, U. S. Schwarz, B. Hoffmann, and R. Merkel. Micropatterned silicone elastomer substrates for high resolution analysis of cellular force patterns. *Rev. Sci. Instrum.* 78:034301, 2007.
- <sup>10</sup>Chetta, J., C. Kye, and S. B. Shah. Cytoskeletal dynamics in response to tensile loading of mammalian axons. *Cytoskeleton (Hoboken)* 67:650–665, 2010.
- <sup>11</sup>Chetta, J., and S. B. Shah. A novel algorithm to generate kymographs from dynamic axons for the quantitative analysis of axonal transport. *J. Neurosci. Methods* 199:230–240, 2011.
- <sup>12</sup>Chun, H., D. S. Lee, and H. C. Kim. Bio-cell chip fabrication and applications. *Methods Mol. Biol.* 509:145–158, 2009.
- <sup>13</sup>Davis, M. J., J. A. Donovan, and J. D. Hood. Stretch-activated single-channel and whole cell currents in vascular smooth muscle cells. *Am. J. Physiol.* 262:C1083–C1088, 1992.
- <sup>14</sup>Folch, A., and M. Toner. Cellular micropatterns on biocompatible materials. *Biotechnol. Prog.* 14:388–392, 1998.
- <sup>15</sup>Formigli, L., E. Meacci, C. Sassoli, R. Squecco, D. Nosi, F. Chellini, F. Naro, F. Francini, and S. Zecchi-Orlandini. Cytoskeleton/stretch-activated ion channel interaction regulates myogenic differentiation of skeletal myoblasts. *J. Cell. Physiol.* 211:296–306, 2007.
- <sup>16</sup>Garvin, J., J. Qi, M. Maloney, and A. J. Banes. Novel system for engineering bioartificial tendons and application of mechanical load. *Tissue Eng.* 9:967–979, 2003.
- <sup>17</sup>Gerstmair, A., G. Fois, S. Innerbichler, P. Dietl, and E. Felder. A device for simultaneous live cell imaging during uni-axial mechanical strain or compression. *J. Appl. Physiol.* 107:613–620, 2009.
- <sup>18</sup>Gilchrist, C. L., S. W. Witvoet-Braam, F. Guilak, and L. A. Setton. Measurement of intracellular strain on deformable substrates with texture correlation. *J. Biomech.* 40:786–794, 2007.
- <sup>19</sup>Hanein, Y., O. Tadmor, S. Anava, and A. Ayali. Neuronal soma migration is determined by neurite tension. *Neuroscience* 172:572–579, 2011.
- <sup>20</sup>Harris, A. K., P. Wild, and D. Stopak. Silicone rubber substrata: a new wrinkle in the study of cell locomotion. *Science* 208:177–179, 1980.
- <sup>21</sup>Haston, W. S., J. M. Shields, and P. C. Wilkinson. The orientation of fibroblasts and neutrophils on elastic substrata. *Exp. Cell Res.* 146:117–126, 1983.
- <sup>22</sup>Hochmuth, R. M. Micropipette aspiration of living cells. *J. Biomech.* 33:15–22, 2000.
- <sup>23</sup>Houtchens, G. R., M. D. Foster, T. A. Desai, E. F. Morgan, and J. Y. Wong. Combined effects of microtopography and cyclic strain on vascular smooth muscle cell orientation. *J. Biomech.* 41:762–769, 2008.
- <sup>24</sup>Huang, L., P. S. Mathieu, and B. P. Helmke. A stretching device for high-resolution live-cell imaging. *Ann. Biomed. Eng.* 38:1728–1740, 2010.
- <sup>25</sup>Jean, R. P., D. S. Gray, A. A. Spector, and C. S. Chen. Characterization of the nuclear deformation caused by changes in endothelial cell shape. *J. Biomech. Eng.* 126:552–558, 2004.
- <sup>26</sup>Kartalov, E. P., W. F. Anderson, and A. Scherer. The analytical approach to polydimethylsiloxane microfluidic technology and its biological applications. *J. Nanosci. Nanotechnol.* 6:2265–2277, 2006.

- <sup>27</sup>Kaunas, R., S. Usami, and S. Chien. Regulation of stretch-induced JNK activation by stress fiber orientation. *Cell. Signal.* 18:1924–1931, 2006.
- <sup>28</sup>Kim, B. S., and D. J. Mooney. Scaffolds for engineering smooth muscle under cyclic mechanical strain conditions. *J. Biomech. Eng.* 122:210–215, 2000.
- <sup>29</sup>Knight, M. M., Z. Bomzon, E. Kimmel, A. M. Sharma, D. A. Lee, and D. L. Bader. Chondrocyte deformation induces mitochondrial distortion and heterogeneous intracellular strain fields. *Biomech. Model. Mechanobiol.* 5:180–191, 2006.
- <sup>30</sup>Koschwanetz, J. H., R. H. Carlson, and D. R. Meldrum. Thin PDMS films using long spin times or tert-butyl alcohol as a solvent. *PLoS ONE* 4:e4572, 2009.
- <sup>31</sup>Lawrence, C. J. The mechanics of spin coating of polymer-films. *Phys. Fluids* 31:2786–2795, 1988.
- <sup>32</sup>Lee, C. F., C. Haase, S. Deguchi, and R. Kaunas. Cyclic stretch-induced stress fiber dynamics—dependence on strain rate, rho-kinase and MLCK. *Biochem. Biophys. Res. Commun.* 401:344–349, 2010.
- <sup>33</sup>Lindqvist, N., Q. Liu, J. Zajadacz, K. Franze, and A. Reichenbach. Retinal glial (muller) cells: Sensing and responding to tissue stretch. *Invest. Ophthalmol. Vis. Sci.* 51:1683–1690, 2010.
- <sup>34</sup>Liu, M., J. R. Sun, Y. Sun, C. Bock, and Q. F. Chen. Thickness-dependent mechanical properties of polydimethylsiloxane membranes. *J. Micromech. Microeng.* 19:035028, 2009.
- <sup>35</sup>Loverde, J. R., V. C. Ozoka, R. Aquino, L. Lin, and B. J. Pfister. Live imaging of axon stretch growth in embryonic and adult neurons. *J. Neurotrauma* 28:2389–2403, 2011.
- <sup>36</sup>Maniotis, A. J., C. S. Chen, and D. E. Ingber. Demonstration of mechanical connections between integrins, cytoskeletal filaments, and nucleoplasm that stabilize nuclear structure. *Proc. Natl. Acad. Sci. USA* 94:849–854, 1997.
- <sup>37</sup>McDonald, J. C., and G. M. Whitesides. Poly(dimethylsiloxane) as a material for fabricating microfluidic devices. *Acc. Chem. Res.* 35:491–499, 2002.
- <sup>38</sup>Merkel, R., N. Kirchgessner, C. M. Cesa, and B. Hoffmann. Cell force microscopy on elastic layers of finite thickness. *Biophys. J.* 93:3314–3323, 2007.
- <sup>39</sup>Mizutani, T., H. Haga, and K. Kawabata. Development of a device to stretch tissue-like materials and to measure their mechanical properties by scanning probe microscopy. *Acta Biomater.* 3:485–493, 2007.
- <sup>40</sup>Norrman, K., A. Ghanbari-Siahkali, and N. B. Larsen. 6 studies of spin-coated polymer films. *Annu. Rep. Sect. C Phys. Chem.* 101:174–201, 2005.
- <sup>41</sup>Paten, J. A., R. Zareian, N. Saeidi, S. A. Melotti, and J. W. Ruberti. Design and performance of an optically accessible, low-volume, mechanobioreactor for long-term study of living constructs. *Tissue Eng. Part C Methods* 17:775–788, 2011.
- <sup>42</sup>Pfister, B. J., A. Iwata, D. F. Meaney, and D. H. Smith. Extreme stretch growth of integrated axons. *J. Neurosci.* 24:7978–7983, 2004.
- <sup>43</sup>Ryu, K. S., X. Wang, K. Shaikh, and C. Liu. A method for precision patterning of silicone elastomer and its applications. *J. Microelectromech. Syst.* 13:568–575, 2004.
- <sup>44</sup>Shah, S. B., and R. L. Lieber. Simultaneous imaging and functional assessment of cytoskeletal protein connections in passively loaded single muscle cells. *J. Histochem. Cytochem.* 51:19–29, 2003.
- <sup>45</sup>Shi, Y., H. Li, X. Zhang, Y. Fu, Y. Huang, P. P. Lui, T. Tang, and K. Dai. Continuous cyclic mechanical tension inhibited runx2 expression in mesenchymal stem cells through rhoa-erk1/2 pathway. *J. Cell. Physiol.* 226:2159–2169, 2011.
- <sup>46</sup>Sia, S. K., and G. M. Whitesides. Microfluidic devices fabricated in poly(dimethylsiloxane) for biological studies. *Electrophoresis* 24:3563–3576, 2003.
- <sup>47</sup>Sleep, J., D. Wilson, R. Simmons, and W. Gratzner. Elasticity of the red cell membrane and its relation to hemolytic disorders: An optical tweezers study. *Biophys. J.* 77:3085–3095, 1999.
- <sup>48</sup>Smith, D. H., J. A. Wolf, T. A. Lusardi, V. M. Lee, and D. F. Meaney. High tolerance and delayed elastic response of cultured axons to dynamic stretch injury. *J. Neurosci.* 19:4263–4269, 1999.
- <sup>49</sup>Smith, D. H., J. A. Wolf, and D. F. Meaney. A new strategy to produce sustained growth of central nervous system axons: continuous mechanical tension. *Tissue Eng.* 7:131–139, 2001.
- <sup>50</sup>Sniatecki, N. J., A. Anguelouch, M. T. Yang, C. M. Lamb, Z. Liu, S. B. Kirschner, Y. Liu, D. H. Reich, and C. S. Chen. Magnetic microposts as an approach to apply forces to living cells. *Proc. Natl. Acad. Sci. USA* 104:14553–14558, 2007.
- <sup>51</sup>Sonobe, T., T. Inagaki, D. C. Poole, and Y. Kano. Intracellular calcium accumulation following eccentric contractions in rat skeletal muscle in vivo: role of stretch-activated channels. *Am. J. Physiol. Regul. Integr. Comp. Physiol.* 294:R1329–R1337, 2008.
- <sup>52</sup>Suresh, S. Biomechanics and biophysics of cancer cells. *Acta Biomater.* 3:413–438, 2007.
- <sup>53</sup>Tondon, A., H. J. Hsu, and R. Kaunas. Dependence of cyclic stretch-induced stress fiber reorientation on stretch waveform. *J. Biomech.* 45:728–735, 2011.
- <sup>54</sup>Venkataraman, S. K., L. Coyne, F. Chambon, M. Gottlieb, and H. H. Winter. Critical extent of reaction of a polydimethylsiloxane polymer network. *Polymer* 30:2222–2226, 1989.
- <sup>55</sup>Wall, M. E., P. S. Weinhold, T. Siu, T. D. Brown, and A. J. Banes. Comparison of cellular strain with applied substrate strain in vitro. *J. Biomech.* 40:173–181, 2007.
- <sup>56</sup>Wang, D., Y. Xie, B. Yuan, J. Xu, P. Gong, and X. Jiang. A stretching device for imaging real-time molecular dynamics of live cells adhering to elastic membranes on inverted microscopes during the entire process of the stretch. *Integr. Biol. (Camb)* 2:288–293, 2010.
- <sup>57</sup>Wang, J. H., and B. Li. Mechanics rules cell biology. *Sports Med. Arthrosc. Rehabil. Ther. Technol.* 2:16, 2010.
- <sup>58</sup>Wang, Y. L., and R. J. Pelham, Jr. Preparation of a flexible, porous polyacrylamide substrate for mechanical studies of cultured cells. *Methods Enzymol.* 298:489–496, 1998.
- <sup>59</sup>Xia, Y. N., and G. M. Whitesides. Soft lithography. *Annu. Rev. Mater. Sci.* 28:153–184, 1998.
- <sup>60</sup>Zhang, H., F. Landmann, H. Zahreddine, D. Rodriguez, M. Koch, and M. Labouesse. A tension-induced mechanotransduction pathway promotes epithelial morphogenesis. *Nature* 471:99–103, 2011.
- <sup>61</sup>Zheng, J., P. Lamoureux, V. Santiago, T. Dennerll, R. E. Buxbaum, and S. R. Heidemann. Tensile regulation of axonal elongation and initiation. *J. Neurosci.* 11:1117–1125, 1991.